


**Near-perfect discrimination of chiral molecules based on steady states of a cavity mode**Yi-Hao Kang <sup>1,2</sup>, Zhe-Ping Lin,<sup>3</sup> Jian-Qun Yang,<sup>4</sup> Jie Song,<sup>1,\*</sup> and Yan Xia<sup>2,5,†</sup><sup>1</sup>*Department of Physics, Harbin Institute of Technology, Harbin 150001, China*<sup>2</sup>*Fujian Key Laboratory of Quantum Information and Quantum Optics (Fuzhou University), Fuzhou 350116, China*<sup>3</sup>*Department of Electronic Information Engineering, Maynooth International Engineering College, Fuzhou University, Fuzhou 350108, China*<sup>4</sup>*School of Materials Science and Engineering, Harbin Institute of Technology, Harbin 150001, China*<sup>5</sup>*Department of Physics, Fuzhou University, Fuzhou 350116, China*

(Received 16 November 2022; revised 23 April 2023; accepted 19 May 2023; published 26 May 2023)

We propose a protocol to realize discrimination of chiral molecules based on steady states of a cavity mode. Using the closed-loop three-level structure of a molecule, an effective Hamiltonian of the molecule-cavity-coupled system is derived. The effective Hamiltonian is similar to a linear driving of the cavity mode, but the driving strength depends on the chirality of the molecule. In the presence of photon loss, the cavity behaves like a driven damped harmonic oscillator, and it will evolve to different steady coherence states according to the chirality of the molecule. By selecting proper parameters, it is possible to obtain steady coherence states with large-enough amplitudes that can be well determined by homodyne measurements on the cavity. Consequently, the chirality of the molecules can be discriminated near perfectly, according to the measurement result of the cavity. Numerical simulations show that the protocol is insensitive to the systematic errors of the control fields and the energy relaxation of the molecules. Therefore, the protocol may provide an effective approach to realize chirality discrimination with high accuracy.

DOI: [10.1103/PhysRevA.107.053714](https://doi.org/10.1103/PhysRevA.107.053714)**I. INTRODUCTION**

Chiral molecules have shown many important applications in chemistry, biotechnologies, and pharmaceuticals [1–4]. For a mirror-symmetrical pair of enantiomers of chiral molecules, they share many physical and chemical properties, but usually possess significantly divergent biological activities and physiological effects [5–8]. Therefore, discriminating the chirality of chiral molecules is a crucial task in the chemical and biological fields.

Conventionally, chirality discrimination can be realized using chemical techniques, such as crystallization and derivatization [9]. However, these chemical techniques are usually time-consuming and expensive. To realize fast and efficient chirality discrimination, much attention has been paid to the optical methods [10–23]. Some early optical methods [10–13] for chirality discrimination is based on the fact that the circularly polarized electromagnetic fields can break mirror symmetry of enantiomers. Because the circularly polarized light interacts with chiral molecules via weak magnetic-dipole and electric-quadrupole interactions [24,25], the chiral signal obtained by such methods is relatively weak. For example, the coupling strength of the magnetic-dipole interaction of the molecule is only about 1/274 of the electric-dipole interaction in Refs. [24,25].

As alternatives, optical methods using linearly polarized light [14–18] have been considered, where the chiral

molecules interact with light through strong electric-dipole interactions [26–29]. Since there exists the sign difference in some of the transition dipole moments, the chirality information can be mapped onto population difference, by subjecting the chiral molecules to an appropriately timed and phased set of electromagnetic fields [19]. Recently, more protocols [19–23] have been proposed based on the electric-dipole interaction. By means of some new quantum control techniques like shortcuts to adiabaticity [30–33] and optimal control [34–37], the speed and accuracy of the chirality discrimination is further improved.

Unfortunately, in a practical physical system for chirality discrimination, there exist several types of experimental imperfections, including the systematic errors in the control fields and the energy relaxation of the molecules [20,21]. When these experimental imperfections are taken into account, it is still challenging to achieve very high accuracy of the chirality discrimination using previous population-based protocols [20–23]. The reasons are as follows. First, the populations of molecules are relatively sensitive to the deviations of the control parameters. For example, in the protocol [20], the error probability of the chirality discrimination reaches about 2% when the strengths of the control pulses have  $\pm 10\%$  relative deviations. Thus, precise control of the parameters is required in the population-based protocols. Second, the excited states of the molecules should be populated in the population-based protocols, but the energy relaxation of the molecules will gradually reduce the populations of the excited states. To obtain an acceptable error probability, long lifetimes of the excited states are required. For example, to obtain error probability lower than 1% using the protocol

\*jsong@hit.edu.cn

†xia-208@163.com

[20], the lifetimes should be 200–300  $\mu\text{s}$ . Such long lifetimes are still hard to be achieved with the current technology. To overcome the shortcomings of the population-based protocols, new attempts [38–41] on the accurate chirality discrimination were made in molecule-cavity coupled systems during the past few years. The results showed that the molecule-cavity coupled systems may be promising candidates for the robust chirality discrimination in the presence of experimental imperfections.

In this paper, we propose an alternative protocol for the accurate discrimination of chiral molecules based on steady states of a cavity mode. The closed-loop three-level structure of the chiral molecule is considered as the physical model. The transition between the ground state and one of the two excited states is coupled with a microwave cavity mode, while that between the ground state and the other excited state is driven by a classical microwave field. In addition, the transition between two excited states is driven by other strong classical microwave fields. Using this physical model, we derive an effective Hamiltonian of the molecule-cavity-coupled system, where the molecule is almost restricted at its ground state and the cavity is similar to a driven harmonic oscillator with the driving strengths depending on the chirality of the molecule. In the presence of photon loss, the cavity behaves like a driven damped harmonic oscillator and its states will converge to different steady coherence states according to the chirality of the molecule. By setting proper parameters, the amplitudes of the steady coherence states are large enough to be distinguished via homodyne measurements on the cavity. Hence, we can obtain the chirality information of the molecule according to the measurement result of the cavity.

We show that the error probability of the homodyne measurements can be described by a complementary error function of the absolute value of the steady-coherence-state amplitude. Thus, the error probability changes slightly when there exist errors in the amplitudes of the steady coherence state, in the large amplitude case. Consequently, the protocol is more insensitive to the experimental imperfections compared with the previous population-based protocols [20–23]. Moreover, since photon loss is used as a physical resource in the protocol, the protocol is also superior to the previous cavity-mode-based protocol [38], where the photon loss is a negative factor.

The performance of the protocol is estimated by the numerical simulations. The results prove that the protocol is robust against the influence of the systematic errors and the energy relaxation of the molecule, in accordance with the theoretical prediction. Therefore, the protocol may provide some useful perspectives for near-perfect chirality discrimination.

The article is organized as follows. In Sec. II, we introduce the physical model for the discrimination of the chiral molecules. In Sec. III, we show the details of the accurate discrimination of chiral molecules based on steady states. In Sec. IV, we perform numerical simulations to estimate the performance of the protocol. Finally, conclusions are given in Sec. V.

## II. PHYSICAL MODEL

We now describe the physical model for the discrimination of the chiral molecules. Considering an enantiomer of chiral

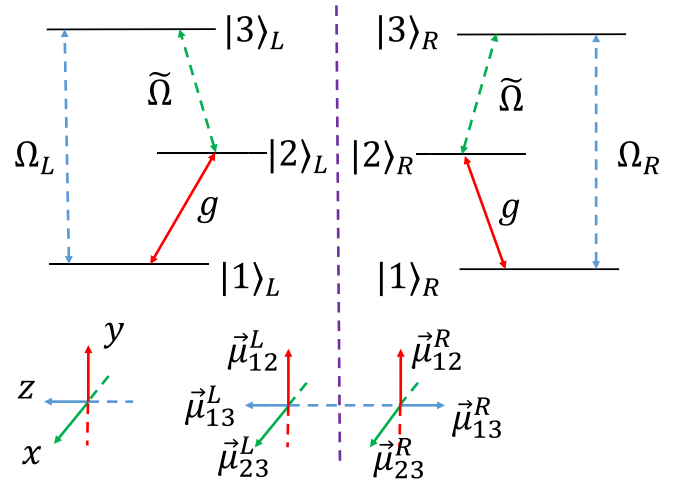


FIG. 1. Comparison of the couplings among three discrete energy states in molecules with left ( $L$ ) and right ( $R$ ) handedness.

molecules with  $s$  handedness ( $s = L, R$ ), it has three discrete energy states  $\{|1\rangle_s, |2\rangle_s, |3\rangle_s\}$ , as shown in Fig. 1. Here,  $L$  and  $R$  correspond to the left and right handedness, respectively. The unit direction vectors of the  $x$ ,  $y$ , and  $z$  axes are assumed as  $\vec{e}_x$ ,  $\vec{e}_y$ , and  $\vec{e}_z$ , respectively. The transition-dipole moments of the transitions  $|1\rangle_s \leftrightarrow |2\rangle_s$  and  $|2\rangle_s \leftrightarrow |3\rangle_s$  are in the same direction for  $L$ - and  $R$ -handed molecules, i.e.,  $\vec{\mu}_{12}^s = \mu_{12}^s \vec{e}_y$ ,  $\vec{\mu}_{23}^s = \mu_{23}^s \vec{e}_x$ . However, the transition-dipole moments of the transition  $|1\rangle_s \leftrightarrow |3\rangle_s$  are in the opposite directions due to the difference of handedness, i.e.,  $\vec{\mu}_{13}^L = -\vec{\mu}_{13}^R = \mu_{13}^s \vec{e}_z$  [19–21].

To realize the chirality discrimination, we couple the transition  $|1\rangle_s \leftrightarrow |2\rangle_s$  resonantly with a microwave cavity mode with the polarization along the  $y$  axis. Assuming that the frequency of the cavity mode is  $\nu$ , the coupling strength is given by  $g = \mu_{12}[\nu/(2\epsilon V)]^{1/2}$ , with  $\epsilon$  and  $V$  the dielectric constant and the volume of the cavity, respectively. Moreover, we apply a classical field

$$\vec{E}'(t) = \tilde{\epsilon} \cos(\tilde{\omega}t) \vec{e}_x, \quad (1)$$

to the molecule, with the frequency  $\tilde{\omega}$  and the amplitude  $\tilde{\epsilon}$ . When the frequency  $\omega_{23}$  of the transition  $|2\rangle_s \leftrightarrow |3\rangle_s$  is equal to the frequency  $\tilde{\omega}$ , the transition  $|2\rangle_s \leftrightarrow |3\rangle_s$  is resonantly driven by the classical field  $\vec{E}'(t)$  with the Rabi frequency

$$\tilde{\Omega} = \tilde{\epsilon} \vec{\mu}_{23}^s \cdot \vec{e}_x / 2 = \tilde{\epsilon} \mu_{23} / 2. \quad (2)$$

In addition, another classical field

$$\vec{E}(t) = \epsilon \cos(\omega t) \vec{e}_z, \quad (3)$$

with the frequency  $\omega$  and the amplitude  $\epsilon$ , is applied to the molecule. When the frequency  $\omega_{13}$  of the transition  $|1\rangle_s \leftrightarrow |3\rangle_s$  is equal to the frequency  $\omega$ , the transition  $|1\rangle_s \leftrightarrow |3\rangle_s$  is resonantly driven by the classical field  $\vec{E}(t)$  with the Rabi frequency

$$\Omega_s = \epsilon \vec{\mu}_{13}^s \cdot \vec{e}_z / 2. \quad (4)$$

From Eq. (4), we find that the Rabi frequencies of the transition  $|1\rangle_s \leftrightarrow |3\rangle_s$  have opposite signs for  $L$ - and  $R$ -handed molecules, i.e.,  $\Omega_L = -\Omega_R = \epsilon \mu_{13} / 2$ . In summary, for both

$L$ - and  $R$ -handed molecules, the total Hamiltonian under the rotating-wave-approximation can be described as

$$H = ga^\dagger|1\rangle_s\langle 2| + \tilde{\Omega}|2\rangle_s\langle 3| + \Omega_s|1\rangle_s\langle 3| + \text{H.c.}, \quad (5)$$

with  $a$  ( $a^\dagger$ ) the annihilation (creation) operator of the cavity mode.

To further construct an effective Hamiltonian, we rewrite the Hamiltonian  $H$  in Eq. (5) by using the vectors  $|\pm\rangle = (|2\rangle_s \pm |3\rangle_s)/\sqrt{2}$  as

$$\begin{aligned} H &= H' + \tilde{H}, \\ H' &= \frac{g}{\sqrt{2}}a^\dagger|1\rangle_s(\langle +| + \langle -|) + \frac{\Omega_s}{\sqrt{2}}|1\rangle_s(\langle +| - \langle -|) + \text{H.c.}, \\ \tilde{H} &= \tilde{\Omega}(\langle +| \langle +| - |-\rangle \langle -|), \end{aligned} \quad (6)$$

where  $\tilde{\Omega}$ ,  $\Omega_s$  and  $g$  are all assumed as real numbers. In the rotating frame of the unitary operator  $R(t) = \exp(-i\tilde{H}t)$ , the Hamiltonian of the system becomes

$$\begin{aligned} H_R(t) &= R^\dagger(t)H'R(t) - iR^\dagger(t)\dot{R}(t) \\ &= \frac{g}{\sqrt{2}}a^\dagger|1\rangle_s(\langle +|e^{-i\tilde{\Omega}t} + \langle -|e^{i\tilde{\Omega}t}) \\ &\quad + \frac{\Omega_s}{\sqrt{2}}|1\rangle_s(\langle +|e^{-i\tilde{\Omega}t} - \langle -|e^{i\tilde{\Omega}t}) + \text{H.c.} \end{aligned} \quad (7)$$

We assume that the molecule is initially prepared in the ground state  $|1\rangle_s$ . Under the condition  $\tilde{\Omega} \gg g, \Omega_s$ , the effective Hamiltonian of the system can be derived via the second-order perturbation theory [42] as

$$H_e = \tilde{\Omega}_s(a + a^\dagger)|1\rangle_s\langle 1|, \quad (8)$$

with  $\tilde{\Omega}_s = -g\Omega_s/\tilde{\Omega}$ .

### III. DISCRIMINATION OF CHIRAL MOLECULES BASED ON STEADY STATES OF CAVITY MODES IN THE PRESENCE OF PHOTON LOSS

In Sec. II, we derive the effective Hamiltonian of the molecule-cavity coupled system. In this section, let us demonstrate that the cavity will finally be stabilized at different steady coherence states in the presence of photon loss if the chirality of the molecules are different.

When the molecule-cavity-coupled system interacts with the environment, there exists two types of decoherence factors in general, the photon loss of the cavity mode and the energy relaxation of the molecule from the excited states to the ground state [20,21]. When the two decoherence factors are taken into account, the evolution of the system (described by the density operator  $\rho$ ) is governed by the master equation as

$$\dot{\rho} = -i[H, \rho] + \kappa\mathcal{L}[a]\rho + \sum_{i=2}^3 \gamma_i\mathcal{L}[\sigma_i^-]\rho, \quad (9)$$

with  $\sigma_i^- = |1\rangle_s\langle i|$  and  $\mathcal{L}[o]\rho = o\rho o^\dagger - (o^\dagger o\rho + \rho o^\dagger o)/2$  ( $o = a, \sigma_i^-$ ). Here,  $\mathcal{L}[a]$  and  $\mathcal{L}[\sigma_i^-]$  denote the superoperators acting on the density operator induced by the photon loss and the energy relaxation from the excited state  $|i\rangle_s$  to the ground state  $|1\rangle_s$ , respectively. In addition,  $\kappa$  is the photon loss rate and  $\gamma_i$  is the energy relaxation rate for the relaxation path  $|i\rangle_s \rightarrow |1\rangle_s$ .

According to the discussions in Sec. II, the effective Hamiltonian of the system is  $H_e$  in Eq. (8) when the molecule is initially in the ground state  $|1\rangle$ . Because  $H_e$  does not excite the molecule to the excited states, the influence of the energy relaxation can be neglected. In this case, the photon loss plays the most important role. Moreover, the density operator of the system can be approximately written by  $\rho = \rho_c \otimes |1\rangle_s\langle 1|$ , with  $\rho_c$  the density operator of the cavity. Thus, the master equation in Eq. (9) is reduced to

$$\dot{\rho} = -i[H_e, \rho] + \kappa\mathcal{L}[a]\rho, \quad (10)$$

in the effective dynamics. The dynamics in Eq. (10) can be considered as the well-known driven damped harmonic oscillator model [43], where the unique steady state of the cavity is the coherent state  $|\alpha_s\rangle_c$  ( $\alpha_s = -2i\tilde{\Omega}_s/\kappa$ ). In fact, substituting  $\rho_c = |\alpha_s\rangle_c\langle \alpha_s|$  into Eq. (10), we have

$$\begin{aligned} -i[H_e, \rho] &= -i\tilde{\Omega}_s(a + a^\dagger)|\alpha_s\rangle_c\langle \alpha_s| \otimes |1\rangle_s\langle 1| \\ &\quad + i\tilde{\Omega}_s|\alpha_s\rangle_c\langle \alpha_s|(a + a^\dagger) \otimes |1\rangle_s\langle 1| \\ &= -i\tilde{\Omega}_s(\alpha_s + a^\dagger)|\alpha_s\rangle_c\langle \alpha_s| \otimes |1\rangle_s\langle 1| \\ &\quad + i\tilde{\Omega}_s|\alpha_s\rangle_c\langle \alpha_s|(a + \alpha_s^*) \otimes |1\rangle_s\langle 1|, \\ \kappa\mathcal{L}[a]\rho &= \frac{\kappa}{2}[2|\alpha_s|^2|\alpha_s\rangle_c\langle \alpha_s| - \alpha_s a^\dagger|\alpha_s\rangle_c\langle \alpha_s| \\ &\quad - \alpha_s^*|\alpha_s\rangle_c\langle \alpha_s|a] \otimes |1\rangle_s\langle 1|, \end{aligned} \quad (11)$$

implying  $-i[H_e, \rho] + \kappa\mathcal{L}[a]\rho = 0$ .

Using the result  $\tilde{\Omega}_s = -g\Omega_s/\tilde{\Omega}$  and  $\Omega_L = -\Omega_R$ , we obtain the following results.

(i) When the molecule is left handed, the cavity will finally be stabilized at the steady coherence state  $|\alpha_L\rangle_c$  with amplitude  $\alpha_L = 2ig\Omega_L/\kappa\tilde{\Omega}$ .

(ii) When the molecule is right handed, the cavity will finally be stabilized at the steady coherence state  $|\alpha_R\rangle_c$  with amplitude  $\alpha_R = -2ig\Omega_R/\kappa\tilde{\Omega}$ .

The coherence states  $|\alpha_L\rangle_c$  and  $|\alpha_R\rangle_c$  are approximately orthogonal when  $\alpha_0 = |\alpha_L| = |\alpha_R|$  is large enough. For example, when  $\alpha_0 = 2.5$ , we obtain  $|\langle \alpha_L|\alpha_R\rangle_c| = \exp(-2\alpha_0^2) \simeq 3.727 \times 10^{-6}$ . In this case, the two coherence states can be well distinguished by using an  $X_\varphi$ -quadrature homodyne measurement [44–47] with a probing mode in the coherence state  $|z\rangle$ , satisfying  $\varphi = \arg(z) = \pi/2$ . The  $X_\varphi$ -quadrature homodyne measurement is equivalent to the eigenprojection  $|x, \varphi\rangle_c\langle x, \varphi|$  of the operator  $X_\varphi = e^{i\varphi}a^\dagger + e^{-i\varphi}a$ . Here, we consider that the measurement results  $x \in [0, +\infty)$  and  $x \in (-\infty, 0)$  correspond to the cavity in the states  $|\alpha_L\rangle_c$  and  $|\alpha_R\rangle_c$ , respectively. Then, the error probability  $P_e$  to distinguish the two coherence states is

$$\begin{aligned} P_e &= \int_0^{+\infty} f_R(x, \varphi)dx = \int_{-\infty}^0 f_L(x, \varphi)dx \\ &= \text{erfc}(\alpha_0)/2, \end{aligned}$$

$$f_s(x, \varphi) = |\langle x, \varphi|\alpha_s\rangle_c|^2 = \frac{1}{\sqrt{\pi}} \exp[-(x - e^{-i\varphi}\alpha_s)^2]. \quad (12)$$

For  $\alpha_0 \geq 2.5$ , the error probability  $P_e \leq 2.0348 \times 10^{-4}$  can be obtained, which means that the discrimination of two coherence states  $|\alpha_L\rangle_c$  and  $|\alpha_R\rangle_c$  is almost deterministic. Therefore, the chirality of molecules can be accurately de-

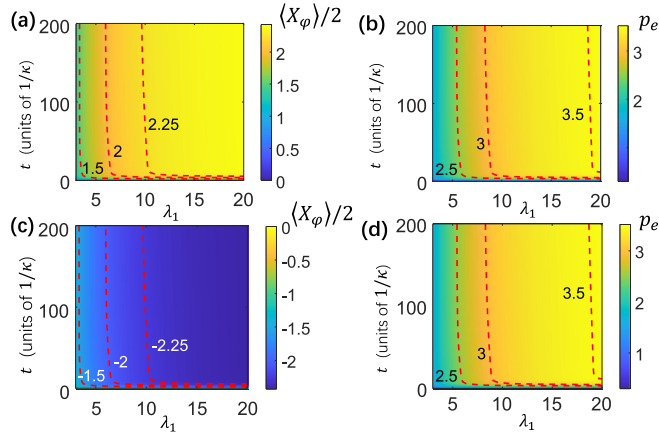


FIG. 2. (a) The average value  $\langle X_\varphi \rangle / 2$  versus  $\lambda_1$  and  $t$  in the case of the left-handed molecule. (b) The logarithm of error probability  $p_e = -\log_{10}(P_e)$  versus  $\lambda_1$  and  $t$  in the case of the left-handed molecule. (c) The average value  $\langle X_\varphi \rangle / 2$  versus  $\lambda_1$  and  $t$  in the case of the right-handed molecule. (d) The logarithm of error probability  $p_e = -\log_{10}(P_e)$  versus  $\lambda_1$  and  $t$  in the case of the right-handed molecule.

terminated according to the measurement result of the cavity mode. In addition, assuming that there exists an error  $\delta\alpha_0 = \alpha'_0 - \alpha_0$ , the change of the error probability is

$$\begin{aligned} \delta P_e &= \{\text{erfc}(\alpha'_0) - \text{erfc}(\alpha_0)\} / 2 \\ &= -\frac{1}{\sqrt{\pi}} \exp(-\alpha_0^2) \delta\alpha_0 + O(\delta\alpha_0^2). \end{aligned} \quad (13)$$

Accordingly, the error probability is almost unchanged if  $\alpha_0$  is large enough. This implies that the protocol is robust against the deviations in the amplitudes of steady coherence states.

#### IV. NUMERICAL SIMULATIONS AND DISCUSSIONS

In this section, let us select proper parameters for the chirality discrimination and estimate the performance of protocol. For simplicity of the discussions, we first use the photon loss rate  $\kappa$  as the reference and set  $g/\kappa = \Omega_L/\kappa = \lambda_1$ ,  $\tilde{\Omega}/\kappa = \lambda_2$ . According to  $\alpha_0 = 2g\Omega_L/\kappa\tilde{\Omega}$ , we derive  $\lambda_2 = 2\lambda_1^2/\alpha_0$ . To obtain a relatively low error probability, we consider  $\alpha_0 = 2.5$ , implying  $\lambda_2 = 0.8\lambda_1^2$ . In general, the ideal steady state is obtained with  $t \rightarrow \infty$ . However, the measurement time cannot be infinite in a real experiment. Therefore, one should also select a finite measurement time  $\tau$  and make sure that the state of the cavity is approximately equal to the ideal steady state at that time. To select proper values of  $\lambda_1$  and  $\tau$ , we plot the average value  $\langle X_\varphi \rangle / 2 = \text{Tr}[X_\varphi \rho] / 2$  and the logarithm of error probability  $p_e = -\log_{10}(P_e)$  versus the parameter  $\lambda_1$  and the evolution time  $t$  in Fig. 2, where the initial state of the cavity is selected as the vacuum state  $|0\rangle_c$ .

In Fig. 2(a),  $\langle X_\varphi \rangle / 2$  versus  $\lambda_1$  and  $t$ , in the case of the left-handed molecule, is shown. Seen from Fig. 2(a), the value of  $\langle X_\varphi \rangle / 2$  tends to 2.5 when  $\lambda_1$  and  $t$  increase. For two different parameters  $\lambda_1 = \tilde{\lambda}_1$  and  $\lambda_1 = \bar{\lambda}_1$  with  $\tilde{\lambda}_1 > \bar{\lambda}_1$ , the increasing speed of  $\langle X_\varphi \rangle / 2$  is faster in the case of  $\lambda_1 = \tilde{\lambda}_1$ . For example, the time to get  $\langle X_\varphi \rangle / 2 \geq 2.25$  is  $t \geq 62.63/\kappa$  when  $\lambda_1 = 10$ , while the time to get  $\langle X_\varphi \rangle / 2 \geq 2.25$  is only  $t \geq 6/\kappa$  when

$\lambda_1 = 15$ . Noticing that  $\langle \alpha_L | X_\varphi | \alpha_L \rangle / 2 = \alpha_0 = 2.5$ , the cavity gradually evolves to the steady state  $|\alpha_L\rangle$  when the average value  $\langle X_\varphi \rangle / 2$  tends to 2.5. Combining with the result shown in Fig. 2(a), we can find that the state of the cavity converges to the steady coherence state  $|\alpha_L\rangle$  with faster speed when a larger parameter  $\lambda_1$  is selected.

In Fig. 2(b), the logarithm of error probability  $p_e = -\log_{10}(P_e)$  versus  $\lambda_1$  and  $t$ , in the case of the left-handed molecule, is shown. Since the error probability decreases when the state of the cavity approach the steady coherence state  $|\alpha_L\rangle$ , the logarithm of the error probability  $p_e = -\log_{10}(P_e)$  increases when  $\lambda_1$  and  $t$  increase, similar to the result shown in Fig. 2(a). According to Fig. 2(b), the evolution time should be longer than  $8/\kappa$  to obtain an error probability  $P_e \leq 10^{-3}$  when  $\lambda_1 = 10$ . In addition, if  $\lambda_1 = 15$  is selected, then the evolution time should be  $t \geq 6/\kappa$  and  $t \geq 8/\kappa$ , for  $P_e \leq 10^{-3}$  and  $P_e \leq 10^{-3.32} = 4.79 \times 10^{-4}$ , respectively. Considering a photon loss rate  $\kappa \simeq 1$  MHz [48], the measurement time  $\tau$  can be selected as 8–10  $\mu\text{s}$  for error probability  $P_e \leq 10^{-3}$  with  $\lambda_1 \geq 10$ . Therefore, the chirality discrimination can be implement rapidly and accurately using the protocol.

In Figs. 2(c) and 2(d), we also study the average value  $\langle X_\varphi \rangle / 2$  and the logarithm of error probability  $p_e = -\log_{10}(P_e)$  versus  $\lambda_1$  and  $t$ , respectively, in the case of the right-handed molecule. Similar to the result in the case of the left-handed molecule, the value of  $\langle X_\varphi \rangle / 2$  tends to  $-2.5$  when  $\lambda_1$  and  $t$  increase. Because of the result  $\langle \alpha_R | X_\varphi | \alpha_R \rangle / 2 = -\alpha_0 = -2.5$ , the state of the cavity converges to the steady coherence state  $|\alpha_R\rangle$  when  $\langle X_\varphi \rangle / 2$  varies to  $-2.5$ . The speed converging to the steady coherence state  $|\alpha_R\rangle$  is faster when the parameter  $\lambda_1$  is greater. When  $\lambda_1 = 10$  and  $\lambda_1 = 15$ , we obtain  $\langle X_\varphi \rangle / 2 \leq -2.25$  with  $t \geq 62.63/\kappa$  and  $t \geq 6/\kappa$ , respectively. The error probability  $P_e$  in the case of the right-handed molecule is also similar to that in the case of the left-handed molecule, i.e.,  $P_e$  decreases when  $\lambda_1$  and  $t$  increase. According to Fig. 2(d), the evolution time to obtain  $P_e \leq 10^{-3}$  is  $t \geq 8/\kappa$  ( $t \geq 6/\kappa$ ) with  $\lambda_1 = 10$  ( $\lambda_1 = 15$ ). Numerical simulation in the case of the right-handed molecule also proves that the chirality discrimination can be near perfectly implemented in a relatively short operation time.

Although the measurement time to obtain the same error probability is shortened by increasing the parameter  $\lambda_1$ , the coupling strength  $g$  and the Rabi frequency  $\Omega$  ( $\tilde{\Omega}$ ) also increase when  $\lambda_1$  increases. Thus, the parameter  $\lambda_1$  should be selected properly to avoid excessive coupling strength and Rabi frequencies. Here, we consider the 1,2-propanediol molecules, where  $|J_{k_-,k_1}\rangle$  is the rotational states with quantum numbers of the limiting prolate ( $k_-$ ) and oblate symmetric top ( $k_1$ ) [49]. The three levels of the molecule in the protocol can be selected as  $|1\rangle_s = |0_{00}\rangle$ ,  $|2\rangle_s = |1_{11}\rangle$ , and  $|3\rangle_s = |1_{10}\rangle$ . In this case, the transition frequencies of  $|1\rangle \leftrightarrow |2\rangle$ ,  $|1\rangle \leftrightarrow |3\rangle$ , and  $|2\rangle \leftrightarrow |3\rangle$  are  $\omega_{12} = 11363$  MHz,  $\omega_{13} = 12212$  MHz, and  $\omega_{23} = 849$  MHz [49], respectively. Considering the photon loss rate  $\kappa = 1$  MHz of a microwave cavity [48], we obtain  $g = \Omega_L = 10$  MHz and  $\tilde{\Omega} = 80$  MHz with  $\lambda_1 = 10$ . The rotating wave approximation is fulfilled as the frequency of the antirotating term is  $\omega_a = 2\omega_{23} = 1698$  MHz, much greater than the Rabi frequency  $\tilde{\Omega}$ . After selecting  $\lambda_1 = 10$ , we select the measurement time as  $\tau = 10 \mu\text{s}$ , so that the error prob-

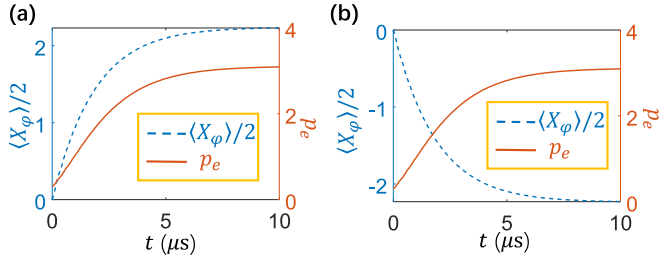


FIG. 3. (a) The average value  $\langle X_\varphi \rangle/2$  and the logarithm of error probability  $p_e = -\log_{10}(P_e)$  versus  $t$  in the case of the left-handed molecule. (b) The average value  $\langle X_\varphi \rangle/2$  and the logarithm of error probability  $p_e = -\log_{10}(P_e)$  versus  $t$  in the case of the right-handed molecule. The parameter  $\lambda_1 = 10$  is selected in the numerical simulations.

ability is lower than  $10^{-4}$  in the  $X_\varphi$ -quadrature homodyne measurement.

Using the selected parameter  $\lambda_1$  and the measurement time  $\tau$ , we plot the variations of the average value  $\langle X_\varphi \rangle/2$  and the logarithm of error probability  $p_e = -\log_{10}(P_e)$  with the evolution time  $t$  in Fig. 3. As shown in Fig. 3(a), we obtain  $\langle X_\varphi \rangle/2 = 2.23$  and  $P_e = 8.0709 \times 10^{-4}$  ( $p_e = 3.09$ ) at  $t = \tau$ , in the case of the left-handed molecule. In addition, according to Fig. 3(b),  $\langle X_\varphi \rangle/2 = -2.23$  and  $P_e = 8.0709 \times 10^{-4}$  ( $p_e = 3.09$ ) is obtained at  $t = \tau$ , in the case of the right-handed molecule. Both results in the cases of the left- and right-handed molecules prove that the cavity will gradually evolve to the steady coherence states predicted by the theory in Sec. III, and the chirality discrimination can be completed with high accuracy in a relatively short time.

In the discussions above, we selected the parameters  $\lambda_1$  and measurement time  $\tau$  according to the results of the numerical simulation. Now, let us further consider some other factors that may influence the performance of the protocol. Here, the case of the left-handed molecule is taken as the example in the following discussions.

Due to the instrument and operation imperfections, there may exist systematic errors in the coupling strength and the Rabi frequencies [34–37]. For the molecule in the protocol, the coupling strength and the Rabi frequencies under the influence of the systematic errors can be described as  $g \rightarrow (1 + \delta_1)g$ ,  $\Omega_s \rightarrow (1 + \delta_2)\Omega_s$ , and  $\tilde{\Omega} \rightarrow (1 + \delta_3)\tilde{\Omega}$ , with  $\delta_k$  ( $k = 1, 2, 3$ ) the systematic error coefficient. To estimate the accuracy of the chirality discrimination in the presence of the systematic errors, we plot the logarithm of error probability  $p_e = -\log_{10}(P_e)$  versus  $\delta_k$  in Fig. 4(a). As shown by the figure, the error probability decreases when  $\delta_1$  ( $\delta_2$ ) is positive and increases when  $\delta_1$  ( $\delta_2$ ) is negative. The highest error probability for  $\delta_1 \in [-0.1, 0.1]$  ( $\delta_2 \in [-0.1, 0.1]$ ) appears at  $\delta_1 = -0.1$  ( $\delta_2 = -0.1$ ) with the result  $P_e = 1.8561 \times 10^{-3}$  ( $P_e = 1.9275 \times 10^{-3}$ ). However, the error probability increases when  $\delta_3$  is positive and decreases when  $\delta_3$  is negative. The highest error probability for  $\delta_3 \in [-0.1, 0.1]$  appears at  $\delta_3 = 0.1$  with the result  $P_e = 1.6282 \times 10^{-3}$ . The trends of the error probability  $P_e$  versus  $\delta_k$  can be easily understood using the result  $\alpha_0 = g\Omega_L/\kappa\tilde{\Omega}$ . When  $\delta_1 > 0$  ( $\delta_2 > 0$ ), the absolute amplitude of the steady coherence state is greater than the value predicted by the theory because the coupling

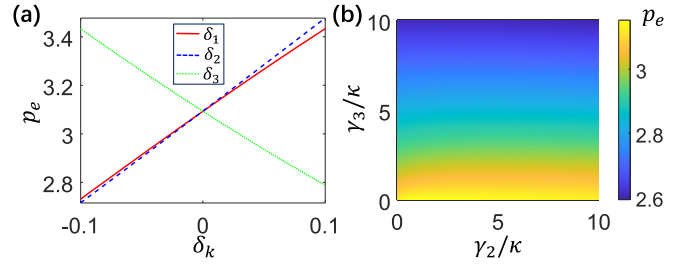


FIG. 4. (a) The logarithm of error probability  $p_e = -\log_{10}(P_e)$  versus systematic error coefficient  $\delta_k$ . (b) The logarithm of error probability  $p_e = -\log_{10}(P_e)$  versus energy relaxation rates  $\gamma_2$  and  $\gamma_3$ . The parameter  $\lambda_1 = 10$  is selected in the numerical simulations and the numerical simulations are performed in the case of the left-handed molecule.

strength  $g$  and the Rabi frequency  $\Omega_L$  are both in the numerator. But the absolute amplitude of the steady coherence state is lower than the predicted value when  $\delta_3 > 0$  because the Rabi frequency  $\tilde{\Omega}$  is in the denominator. As the error probability  $P_e$  has a negative correlation with the absolute amplitude  $\alpha_0$  of the steady coherence states, we can know the variation of the error probability  $P_e$  by analyzing the deviation of the absolute amplitude  $\alpha_0$ . In addition, we can also find from Fig. 4(a) that the error probability remains at the level of  $10^{-3}$  when the systematic error rates is about  $\pm 10\%$ . Therefore, the protocol is insensitive to the systematic errors in the coupling strength and the Rabi frequencies.

In the above discussions, we omit the influence of the energy relaxation of the molecule, as the molecule almost remains in the ground state  $|1\rangle_s$  under the effective dynamics governed by the effective Hamiltonian  $H_e$  in Eq. (8). To confirm that the influence of the energy relaxation to the chirality discrimination is small, we perform the numerical simulation based on the full master equation shown in Eq. (9). The logarithm of error probability  $p_e = -\log_{10}(P_e)$  versus energy relaxation rates  $\gamma_2$  and  $\gamma_3$  are plotted in Fig. 4(b). Seen from Fig. 4(b), the error probability is insensitive to the energy relaxation from the excited state  $|2\rangle_s$ . When  $\gamma_2 \leq 10\kappa$  and  $\gamma_3 = 0$ , the highest error probability appears at  $\gamma_2 = 0$ , where the error probability is  $P_e = 8.0705 \times 10^{-4}$ . However, the lowest error probability appears at  $\gamma_2 = \kappa$ , where the error probability is  $P_e = 7.0291 \times 10^{-4}$ . The lowest probability does not appear at  $\gamma_2 = 0$  because the energy relaxation also prevents the molecule from being excited to the excited state  $|2\rangle_s$ . Therefore, the energy relaxation of the molecule from the excited state  $|2\rangle_s$  may even help to improve the performance of the protocol with proper energy relaxation rate  $\gamma_2$ .

The error probability is more sensitive to the energy relaxation from the excited state  $|3\rangle_s$  compared with that from the excited state  $|2\rangle_s$ . When  $\gamma_2 = 0$  and  $\gamma_3 \leq 10\kappa$ , the highest (lowest) error probability is  $P_e = 2.5032 \times 10^{-3}$  ( $P_e = 8.0705 \times 10^{-4}$ ), appearing at  $\gamma_3 = 10\kappa$  ( $\gamma_3 = 0$ ). When the energy relaxation rate varies from  $\gamma_3 = 0$  to  $\gamma_3 = 10\kappa$  with  $\gamma_2 = 0$ , the change of the error probability is lower than  $1.6961 \times 10^{-3}$ . Consequently, the chirality discrimination is also robust against the energy relaxation of the molecule from the excited state  $|3\rangle_s$ .

Considering the energy relaxation from both the excited states  $|2\rangle_s$  and  $|3\rangle_s$ , with the energy relaxation rates in the range  $\{\gamma_2, \gamma_3\} \in [0, 10\kappa]$ , the error probability is still lower than  $2.5609 \times 10^{-3}$ . In the worst case, we have  $\gamma_2 = \gamma_3 = 10\kappa = g$ . This means that the protocol still works well even when the energy relaxation rates are comparable with the coupling strength. Accordingly, the chirality discrimination can still be implemented accurately when the energy relaxation of the molecules is taken into account.

## V. CONCLUSION

In conclusion, we proposed a protocol for accurate discrimination of chiral molecules based on steady states of a cavity mode. The closed-loop three-level structure, with the transition between the excited states of the molecule driven by a relatively strong microwave field was exploited to build a chirality-dependent effective Hamiltonian of the molecule-cavity-coupled system. Governed by the effective Hamiltonian, the molecule is almost restricted in its ground state, while the cavity behaves like a driven harmonic oscillator with the driving strengths depending on the chirality of the molecule. When the photon loss of the cavity is taken into account, the dynamics of the system is similar to the driven damped harmonic oscillator model. In this case, the state of the cavity will finally converge to steady coherence states with opposite amplitudes, according to the chiralities of the molecules. By setting proper parameters, the amplitudes of the steady coherence states, in the cases of left- and right-handed molecules, are large enough to be distinguished via homodyne measurements on the cavity. Consequently, we can determine the chirality of the molecule through the measurement result of the cavity.

We notice that the error probability  $P_e$  of the homodyne measurement is the complementary error function of the absolute amplitude  $\alpha_0$  of the steady coherence states, i.e.,  $P_e = \text{erfc}[\alpha_0]/2$ . The error probability is insensitive to the deviation of  $\alpha_0$ , if  $\alpha_0$  is large enough. As a result, the error probability changes slightly when the steady states deviates from the ideal one due to the experimental imperfections, including the systematic errors of the control parameters and the energy relaxation of the molecule. Therefore, the chirality discrimination retains high accuracy under the influence of the experimental imperfections. These results are also proved by the numerical simulations in Sec. IV.

Compared with the previous chirality discrimination protocols [20–23] based on the population difference of the molecules, the present protocol is robust against experimental imperfections. This is because the populations of the molecules generally vary significantly when the control parameters change. Moreover, as the excited states of the molecules should be populated in the population-based protocols, such protocols are also more insensitive to the energy relaxation of the molecules.

In addition, the present protocol is superior to the previous chirality discrimination protocol [38] based on the cavity mode. In the previous protocol [38], the evolution of the cavity is based on the unitary evolution. However, due to

the influence of photon loss, the unitary evolution is spoiled. As a result, the chirality discrimination in the protocol [38] is relatively sensitive to the influence of photon loss. Since photon loss of the cavity is inevitable in a real experiment, the accuracy of the previous protocol [38] is limited. In the present protocol, rather than a negative factor, the photon loss is used as a physical resource to obtain the steady coherence states of the cavity. Accordingly, the present protocol may be more easily implemented in experiments and the accuracy of the chirality discrimination should be higher than that using unitary evolution.

Furthermore, in the present protocol, the effective Hamiltonian is constructed by using a relatively strong microwave field to drive the transition between the excited states of the molecule. The second-order perturbation theory was only used once in the derivation of the effective Hamiltonian and the Stark shift terms were completely eliminated. However, in the previous protocol [38], the effective Hamiltonian was derived based on the large detuning condition. The second-order perturbation theory was used twice in the derivation of the effective Hamiltonian and there existed extra Stark shift terms to be dealt with. Therefore, the effective coupling strength in the previous protocol [38] is weaker than that in the present protocol. Moreover, the extra Stark shift terms in the previous protocol [38] were also related to the phase in the complex amplitude of the coherence state. This makes the chirality discrimination in the previous protocol [38] more sensitive to parameter errors since the phase of the probing mode of the homodyne measurement should match with the phase of the cavity mode. Therefore, the present protocol is more robust against parameter errors compared with the previous protocol [38]. According to the advantages shown above, we believe the protocol can be feasible to realize near-perfect chirality discrimination against experimental imperfection.

To implement the chirality discrimination of many molecules, we may apply the device demonstrated in Ref. [49]. The device contains a cryogenic cell with an embedded cavity. The molecules are gradually injected into the device from a feed tube. When a molecule is injected, it will be cooled down to its rotational temperature by a cold helium buffer gas. Then, we will drive the injected molecule with classical fields. Consequently, the cavity mode can evolve to a coherence state and be measured by a homodyne measurement. After that, the molecule will get out of the cavity and arrive at a cold wall of the device and finally freeze there. In addition, the state of the cavity is reset to the vacuum state using a linear drive of the cavity. Then the next molecule is injected and we repeat the above operations. In this way, the chirality discrimination of many molecules can be realized.

## ACKNOWLEDGMENTS

This work was supported by the National Natural Science Foundation of China under Grants No. 11575045, No. 11674060, and No. 11874114; the Natural Science Funds for Distinguished Young Scholar of Fujian Province under Grant No. 2020J06011; and Project from Fuzhou University under Grant No. JG202001-2.

- [1] J. Gal, *Chirality* **24**, 959 (2012).
- [2] A. R. Ribeiro, P. M. L. Castro, and M. E. Tiritan, *Environmental Chemistry Letters* **10**, 239 (2012).
- [3] K. T. Barrett, A. J. Metrano, P. R. Rablen, and S. J. Miller, *Nature (London)* **509**, 71 (2014).
- [4] C. L. Amorim, I. S. Moreira, A. R. Ribeiro, L. H. Santos, C. Delerue-Matos, M. E. Tiritan, and P. M. Castro, *International Biodeterioration & Biodegradation* **115**, 277 (2016).
- [5] N. P. Franks and W. R. Lieb, *Science* **254**, 427 (1991).
- [6] C. Vogt and S. Kiessig, *J. Chromatogr., A* **745**, 53 (1996).
- [7] K. Bodenhöfer, A. Hierlemann, J. Seemann, G. Gauglitz, B. Koppenhoefer, and W. Gpel, *Nature (London)* **387**, 577 (1997).
- [8] S. Eibenberger, J. Doyle, and D. Patterson, *Phys. Rev. Lett.* **118**, 123002 (2017).
- [9] *Chiral Separation Methods for Pharmaceutical and Biotechnological Products*, edited by S. Ahuja (John Wiley & Sons, New York, 2010).
- [10] L. A. Nafie, T. A. Keiderling, and P. J. Stephens, *J. Am. Chem. Soc.* **98**, 2715 (1976).
- [11] C. Lux, M. Wollenhaupt, T. Bolze, Q. Liang, J. Köhler, C. Sarpe, and T. Baumert, *Angew. Chem., Int. Ed.* **51**, 4755 (2012).
- [12] C. S. Lehmann, N. B. Ram, I. Powis, and M. H. M. Janssen, *J. Chem. Phys.* **139**, 234307 (2013).
- [13] R. E. Goetz, T. A. Isaev, B. Nikoobakht, R. Berger, and C. P. Koch, *J. Chem. Phys.* **146**, 024306 (2017).
- [14] M. Shapiro, E. Frishman, and P. Brumer, *Phys. Rev. Lett.* **84**, 1669 (2000).
- [15] P. Brumer, E. Frishman, and M. Shapiro, *Phys. Rev. A* **65**, 015401 (2001).
- [16] D. Gerbasi, M. Shapiro, and P. Brumer, *J. Chem. Phys.* **115**, 5349 (2001).
- [17] P. Král and M. Shapiro, *Phys. Rev. Lett.* **87**, 183002 (2001).
- [18] P. Král, I. Thanopoulos, M. Shapiro, and D. Cohen, *Phys. Rev. Lett.* **90**, 033001 (2003).
- [19] N. V. Vitanov and M. Drewsen, *Phys. Rev. Lett.* **122**, 173202 (2019).
- [20] J.-L. Wu, Y. Wang, J. Song, Y. Xia, S.-L. Su, and Y.-Y. Jiang, *Phys. Rev. A* **100**, 043413 (2019).
- [21] J.-L. Wu, Y. Wang, J.-X. Han, C. Wang, S.-L. Su, Y. Xia, Y. Jiang, and J. Song, *Phys. Rev. Applied* **13**, 044021 (2020).
- [22] J.-L. Wu, Y. Wang, S.-L. Su, Y. Xia, Y. Jiang, and J. Song, *Opt. Express* **28**, 33475 (2020).
- [23] W.-W. Ding, Y.-H. Kang, Y. Liu, J. Song, B.-H. Huang, and Y. Xia, *Ann. Phys. (Leipzig)* **534**, 2100573 (2022).
- [24] A. Salam and W. J. Meath, *J. Chem. Phys.* **106**, 7865 (1997).
- [25] A. Salam and W. Meath, *Chem. Phys.* **228**, 115 (1998).
- [26] Y. Fujimura, L. González, K. Hoki, J. Manz, and Y. Ohtsuki, *Chem. Phys. Lett.* **306**, 1 (1999).
- [27] L. González, D. Kröner, and I. R. Solá, *J. Chem. Phys.* **115**, 2519 (2001).
- [28] K. Hoki, L. González, and Y. Fujimura, *J. Chem. Phys.* **116**, 8799 (2002).
- [29] D. Kröner, M. F. Shibl, and L. González, *Chem. Phys. Lett.* **372**, 242 (2003).
- [30] M. Demirplak and S. A. Rice, *J. Phys. Chem. A* **107**, 9937 (2003).
- [31] X. Chen, I. Lizuain, A. Ruschhaupt, D. Guéry-Odelin, and J. G. Muga, *Phys. Rev. Lett.* **105**, 123003 (2010).
- [32] X. Chen, E. Torrontegui, and J. G. Muga, *Phys. Rev. A* **83**, 062116 (2011).
- [33] B.-H. Huang, Y.-H. Kang, Y.-H. Chen, Q.-C. Wu, J. Song, and Y. Xia, *Phys. Rev. A* **96**, 022314 (2017).
- [34] A. Ruschhaupt, X. Chen, D. Alonso, and J. G. Muga, *New J. Phys.* **14**, 093040 (2012).
- [35] D. Daems, A. Ruschhaupt, D. Sugny, and S. Guérin, *Phys. Rev. Lett.* **111**, 050404 (2013).
- [36] Y.-H. Kang, Z.-C. Shi, J. Song, and Y. Xia, *Phys. Rev. A* **102**, 022617 (2020).
- [37] Y.-H. Kang, J. Song, and Y. Xia, *Opt. Lett.* **47**, 4099 (2022).
- [38] Y.-H. Kang, Z.-C. Shi, J. Song, and Y. Xia, *Opt. Lett.* **45**, 4952 (2020).
- [39] B. Liu, C. Ye, C. P. Sun, and Y. Li, *Phys. Rev. A* **104**, 013113 (2021).
- [40] Y.-Y. Chen, J.-J. Cheng, C. Ye, and Y. Li, *Phys. Rev. Res.* **4**, 013100 (2022).
- [41] F. Zou, Y.-Y. Chen, B. Liu, and Y. Li, *Opt. Express* **30**, 31073 (2022).
- [42] D. F. James and J. Jerke, *Can. J. Phys.* **85**, 625 (2007).
- [43] V. V. Albert, C. Shu, S. Krastanov, C. Shen, R.-B. Liu, Z.-B. Yang, R. J. Schoelkopf, M. Mirrahimi, M. H. Devoret, and L. Jiang, *Phys. Rev. Lett.* **116**, 140502 (2016).
- [44] K. Nemoto and W. J. Munro, *Phys. Rev. Lett.* **93**, 250502 (2004).
- [45] S. D. Barrett, P. Kok, K. Nemoto, R. G. Beausoleil, W. J. Munro, and T. P. Spiller, *Phys. Rev. A* **71**, 060302(R) (2005).
- [46] J. M. Torres, J. Z. Bernád, and G. Alber, *Phys. Rev. A* **90**, 012304 (2014).
- [47] C. A. González-Gutiérrez and J. M. Torres, *Phys. Rev. A* **99**, 023854 (2019).
- [48] Z.-L. Xiang, S. Ashhab, J. Q. You, and F. Nori, *Rev. Mod. Phys.* **85**, 623 (2013).
- [49] D. Patterson, M. Schnell, and J. M. Doyle, *Nature (London)* **497**, 475 (2013).